

Absence of Long-Range Coherence in the Parametric Emission from Photonic Wires

M. Wouters^{1,2} and I. Carusotto¹

¹*BEC-CNR-INFM and Dipartimento di Fisica, Università di Trento, I-38050 Povo, Italy*

²*TFVS, Universiteit Antwerpen, Universiteitsplein 1, 2610 Antwerpen, Belgium*

We analytically investigate the spatial coherence properties of the signal emission from one-dimensional optical parametric oscillators. Because of the reduced dimensionality, quantum fluctuations are able to destroy the long-range phase coherence even far above threshold. The spatial decay of coherence is exponential and, for realistic parameters of semiconductor photonic wires in the strong exciton-photon coupling regime, it is predicted to occur on an experimentally accessible length scale.

PACS numbers: 42.25.Kb, 42.65.Yj, 71.36.+c, 89.75.Kd

I. INTRODUCTION

A central concept in the theory of nonlinear dynamical systems is the so-called pattern formation phenomenon, where a spatially ordered structure appears in an otherwise homogeneous system when this is driven far from thermodynamical equilibrium¹. Very important examples of pattern formation are found in the transverse dynamics of nonlinear optical systems^{2,3}, e.g. lasers, bistable devices, as well as planar optical parametric oscillators (OPOs).

In OPOs, the pattern formation phenomenon manifests itself as the appearance of two additional coherent beams, called the signal and the idler, originating from nonlinear conversion of the pump beam when its intensity is brought beyond a threshold value⁴. An interesting point of view on OPO operation is provided by the analogy with the Bose-Einstein condensation phenomenon of equilibrium statistical mechanics⁵: as it happens for the matter Bose field in the condensate mode when the temperature is lowered below the condensation temperature, the population of the signal/idler modes becomes macroscopic above the threshold and the field becomes coherent. Although many aspects of the OPO operation are successfully interpreted in terms of concepts of equilibrium statistical mechanics^{6,7}, care has to be paid as a non-equilibrium steady state is fundamentally different from a thermodynamical equilibrium state: it is in fact determined by a dynamical equilibrium between external driving and dissipation and does not follow a simple thermal Boltzmann law^{8,9}.

At equilibrium, it is well known that long-wavelength fluctuations of both thermal and quantum origin can destroy long-range phase coherence in reduced dimensionality Bose systems, thus replacing true Bose-Einstein condensates with quasi-condensates^{5,10,11}. First studies for the non-equilibrium case have been recently published in an optical context^{7,12,13} pointing out several analogies with the equilibrium case, but the peculiarities of the non-equilibrium case have not been fully appreciated yet nor experimentally investigated.

The aim of the present paper is to obtain analytical predictions for the long-range coherence properties of

the parametric emission from one-dimensional photonic wires. Although the theory that we develop for reduced-dimensionality effects in non-equilibrium systems is a general one and can be extended to a large class of physical systems showing non-equilibrium phase transitions and pattern formation, our attention will be focussed on a specific example of solid-state system in which the effects we predict are experimentally accessible with the current semiconductor technology.

II. THE PHYSICAL SYSTEM

We consider planar semiconductor microcavities in the strong-coupling regime^{14,15}, a system in which OPO operation has been recently observed^{16,17}. The extremely large value of the excitonic nonlinearity is responsible for the ultra-low OPO threshold of these systems, which suggests an enhanced role of quantum fluctuations. By nanostructuring planar cavities, reduced dimensionality *photonic wires* can be obtained without spoiling the strong-coupling condition, nor the possibility of OPO operation¹⁸. All these facts make these systems an ideal candidate for the study of quantum effects on pattern formation in non-equilibrium systems, in particular low-dimensional ones.

A schematic plot of a photonic wire is given in Fig.1a: light is confined in the growth z direction and in the transverse y direction by respectively the DBR mirrors and the lateral etching of the structure. On the other hand, it is free to propagate along the longitudinal x direction. The photonic states are then classified¹⁸ by the longitudinal wave vector k , the subband index j and the polarization index $\sigma = \{\parallel, \perp\}$, and can be used as a basis over which to expand the (vectorial) electric field operator:

$$\hat{\mathbf{E}}(x, y, z) = \sum_{j\sigma} \int \frac{dk}{2\pi} \hat{a}_{kj\sigma} \mathbf{E}_{kj\sigma}(y, z) e^{ikx}. \quad (1)$$

The polarization and spatial profile of the mode $\mathbf{E}_{kj\sigma}(y, z)$ depends on the details of the specific structure and has to be computed by solving Maxwell's equations for the specific geometry under consideration. Generally,

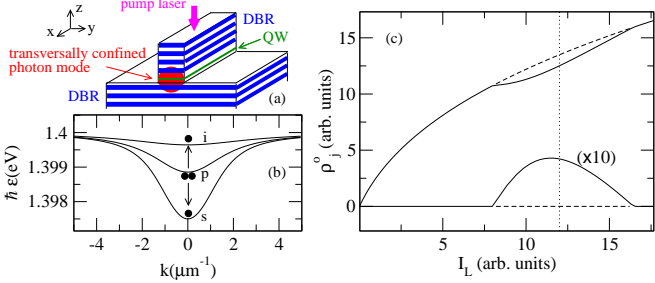


FIG. 1: (a) Sketch of a semiconductor photonic wire with an embedded quantum well (QW). Confinement in the z, y directions is provided by respectively a pair of Distributed Bragg Reflectors (DBR) and a lateral etching of the cavity. (b) Linear regime dispersions of signal, pump and idler subbands and sketch of the parametric process under examination. (c) Exciton density in the pump and signal modes as a function of the pump laser intensity for a given $\hbar\omega_p = 1.398725$ eV. Full (dashed) lines represent linearly stable (unstable) solutions. Cavity parameters inspired by Ref.18: $\hbar\omega_C = \hbar\omega_X = 1.4$ eV, $k_z = 20\mu\text{m}^{-1}$, $\hbar\Omega_R = 2.5$ meV, $L_y = 4\mu\text{m}$, $\hbar g = 5 \times 10^{-6}$ eV μm^2 and $\hbar\gamma_{s,p,i} = 0.15$ meV.

it will show a non-trivial spatial and polarization structure¹⁹. As a function of the longitudinal wavevector k the dispersion of the $j\sigma$ subband is approximately given¹⁸ by

$$\omega_{C,j\sigma}(k) = \omega_{C,j\sigma}^0 \sqrt{1 + (k^2 + k_{y,j\sigma}^2)/k_{z,j\sigma}^2}, \quad (2)$$

where $k_{y,j\sigma}$ and $k_{z,j\sigma}$ are the quantized photon wavevectors in respectively the y and z directions.

The strong dipole coupling between cavity photons and the quantum well exciton results in a Rabi frequency Ω_R larger than the damping rates so that the eigenmodes of the system at linear regime are polaritons, i.e. coherent superpositions of cavity-photonic and excitonic modes. Compared to the photonic one (2), the dispersion of the exciton is negligible, so that the excitonic response can be safely considered as being local. As a consequence, each photonic subband only mixes with the excitonic state of wavefunction $\mathbf{E}_{k,j\sigma}(y, z = z_{QW})$, z_{QW} being the position of the quantum well³¹.

An example of the polaritonic dispersion $\varepsilon_j(k)$ of the three lowest s, p, i subbands is plotted in Fig.1b for realistic experimental parameters. For each subband, only a single polarization state is considered here: as experimentally shown in Ref. 18, the splitting between the $\sigma = \parallel, \perp$ polarization states in photonic wires is in fact large enough for the parametric process to select a single polarization state, while the other one can be safely neglected.

Polaritons are injected into the cavity by means of a coherent and monochromatic pump laser incident on the cavity at a frequency ω_L close to resonance with the central p subband. In order to exclusively inject $k = 0$ polaritons into the p subband, the laser field amplitude has

to be constant along the x direction and to have a negligible overlap in the y direction with all subbands but for the p one. A possible choice to fulfill both conditions, is to use a wide laser beam incident on the sample along the yz plane at an angle chosen in such a way to match the quantized k_y wavevector of the p subband.

Because of the nonlinearity due to exciton-exciton interactions within the quantum well, two *pump* polaritons in the p subband are then parametrically converted into one *signal* polariton in the s subband and one *idler* polariton in the i subband.

III. THE THEORETICAL MODEL

As discussed in detail in Ref.7, a simple, yet quantitative description of the dynamics of the polariton quantum field in a microcavity is based on a Wigner representation of the quantum fields in terms of classical, yet *stochastic* **C**-number polariton fields. As the parametric dynamics is concentrated in the three s, p, i subbands, it is useful to project the polariton field onto these modes, so to restrict our analysis to three one-dimensional polaritonic fields $\phi_{s,p,i}(x)$. Within the Wigner framework³², the time-evolution of the fields $\phi_{s,p,i}(x)$ is described by stochastic differential equations, whose form in Fourier space is:

$$\begin{aligned} i d\phi_j(k) = & \left\{ \left[\varepsilon_j(k) - \frac{i}{2} \gamma_j(k) \right] \phi_j(k) + \right. \\ & + 2\pi \delta_{jp} \delta(k) F_L e^{-i\omega_L t} + \\ & + \sum_{j'} \int \frac{dk'}{2\pi} \mathcal{E}_{jj'}(k, k') \phi_{j'}(k') \right\} dt + \\ & + \sqrt{\frac{\gamma_j(k)}{4}} dW_j(k, t). \quad (3) \end{aligned}$$

As discussed in the previous section, the incident laser coherently drives the pump subband p with an amplitude F_L . The damping rates $\gamma_j(k)$ accounts for radiative and non-radiative losses of both the excitonic and photonic components of the polaritons. In the region of interest³³, they have a weak dependence on k . In agreement with the fluctuation-dissipation theorem²⁰, damping is intimately connected to quantum fluctuations. These show up in the Wigner formalism as Gaussian, complex-valued, white noise terms $dW_j(k, t)$ satisfying

$$\overline{dW_j(k, t) dW_{j'}(k', t)} = 0 \quad (4)$$

$$\overline{dW_j(k, t) dW_{j'}^*(k', t)} = 4\pi dt \delta(k - k') \delta_{jj'}. \quad (5)$$

Expectation values of symmetrically-ordered observables are then obtained as averages of the corresponding **C**-number quantity over the noise $dW_j(x, t)$.

The nonlinear coupling responsible for the parametric process comes from the collisional exciton-exciton interactions in the quantum well. All other nonlinear processes are in fact much weaker and do not contribute

in a significant way to the dynamics of the system. At the simplest level, exciton-exciton collisional interactions can be modelled by a polarization-independent, repulsive contact potential with strength $g > 0^{14,15}$.

Under the hypothesis that the polaritonic dynamics is restricted to the s, p, i subbands of the lower polariton, the mean-field polariton-polariton interaction energy can be written as

$$\mathcal{E}_{jj'}(k, k') = \sum_{r,s} \int \frac{dp}{2\pi} g_{1D}^{jrj's} \phi_r^*(p - k) \phi_s(p - k'), \quad (6)$$

where the overlap integrals of the excitonic component of the transverse wave functions of the different subbands are defined as:

$$g_{1D}^{jrj's} = g \int dy \phi_{X\perp}^{j*}(y) \phi_{X\perp}^{r*}(y) \phi_{X\perp}^{j'}(y) \phi_{X\perp}^s(y). \quad (7)$$

The transverse excitonic wavefunctions $\phi_{X\perp}^j(y)$ are proportional to $\mathbf{E}_{kj\sigma}(y, z = z_{QW})$ and normalized to the excitonic Hopfield weight of the subband:

$$\int dy |\phi_{X\perp}^j(y)|^2 = |U_X^j|^2. \quad (8)$$

For the sake of notational simplicity, we have not explicitly indicated the k -dependence of the transverse wavefunction $\phi_{X\perp}^j(y)$: given the small range of wavevectors k involved in the parametric emission (of the order of the inverse coherence length $1/\ell_c$), it can be safely neglected in the following.

The generalization of (7) to the case of spin-dependent exciton-exciton interactions is straightforward: in this case, the scalar coupling constant g has to be replaced by a four-indices tensor^{21,22} which is to be contracted with the four (vectorial) excitonic wavefunctions $\phi_{X\perp}^j(y)$.

IV. MEAN-FIELD

The *mean-field* solution of the motion equations (3) once the noise terms are neglected has the simple plane wave structure:

$$\phi_j^o(x) = \sqrt{\rho_j^o} e^{i(k_j x - \omega_j t + \theta_j)}. \quad (9)$$

At low pump intensities, a stable solution with a finite density in the pump mode only (i.e. $\rho_s^o = \rho_i^o = 0$) exists. The wavevector $k_p = 0$, as well as the frequency $\omega_p = \omega_L$ are fixed by the external laser; in particular, we have chosen ω_L to be just below the bottom of the p subband so as to avoid complicated pump bistability effects^{23,24,25}. For increasing pump powers, this solution eventually becomes dynamically unstable above some threshold, and is replaced by a new solution with finite signal and idler intensities $\rho_{s,i}^o$. The pump frequency and wavevector remain the same $\omega_p = \omega_L$ and $k_p = 0$,

while many values are possible for the signal/idler frequencies $\omega_{s,i}$ and wavevectors $k_{s,i}$, with the only constraint that $\omega_i = 2\omega_L - \omega_s$ and $k_i = -k_s$ and that the solution is dynamically stable. This latter condition defines a band¹ of stable k_s values and for each of them, the densities $\rho_{s,p,i}^o$ and the frequencies $\omega_{s,i}$ can be simply obtained by substituting the ansatz (9) into the deterministic part of the motion equation (3). While the phase θ_p of the pump field is fixed by the one of the incident laser, the signal and idler ones $\theta_{s,i}$ remain free, with only a constraint on their sum $\theta_s + \theta_i$. The phase rotation $\theta_{s,i} \rightarrow \theta_{s,i} \pm \Delta\theta$ is in fact a symmetry of the problem, a $U(1)$ symmetry which is spontaneously broken²⁶ above the parametric threshold by the solution (9).

The results for the signal, pump, and idler densities $\rho_{s,p,i}^o$ are plotted in Fig.1c as a function of the pump laser intensity $I_L = |F_L|^2$ for the specific case of a signal wavevector $k_s = 0$, which is the first to become unstable for the chosen parameters. The results would however be qualitatively similar if a finite $k_s \neq 0$ was taken. The signal/idler densities $\rho_{s,i}^o$ continuously grow from zero starting from the lower threshold, get to their maximum value, and then go back to zero at the upper threshold, where we are back to a pump-only mean-field solution $\rho_s^o = \rho_i^o = 0^{24,25}$.

V. BOGOLIUBOV THEORY

The simplest way to include the effect of noise terms is to linearize the Wigner equation (3) around the mean-field solution (9) and treat the noise as a perturbation. This is best done using the same ansatz:

$$\phi_j(x, t) = \sqrt{\rho_j^o + \delta\rho_j(x, t)} e^{i(k_j x - \omega_j t + \theta_j + \delta\theta_j(x, t))}. \quad (10)$$

as in the generalized density-phase Bogoliubov theory developed for the study of quasi-condensates at equilibrium^{10,11}. This approach does not require the existence of long-distance coherence, but only that density fluctuations are small $|\delta\rho_j| \ll \rho_j^o$, and the signal and idler phases are well defined and locally locked by the parametric process $|2\delta\theta_p - \delta\theta_s - \delta\theta_i| \ll 1$.

Simple Ito manipulations of (3), lead to the linearized motion equation for the fluctuations in frequency space:

$$\omega \mathcal{U}(k, \omega) = \mathcal{L}(k) \mathcal{U}(k, \omega) + \sqrt{\Gamma(k)/4} \mathcal{W}(k, \omega). \quad (11)$$

The fluctuation 6-vector is defined as $\mathcal{U}(k, \omega) = [\mathbf{u}^{(+)}(k, \omega), \mathbf{u}^{(-)}(k, \omega)]^T$, with the 3-vector:

$$\mathbf{u}_m^{(\pm)}(k, \omega) = \frac{\delta\rho_m(k, \omega)}{2\sqrt{\rho_m^o}} \pm i\sqrt{\rho_m^o} \delta\theta_m(k, \omega). \quad (12)$$

The index m takes here the values 1, 2, 3 corresponding respectively to the subbands s, p, i . The complex-valued noise 6-vector is analogously defined as $\mathcal{W}(k, \omega) = [\mathbf{w}(k, \omega), -\mathbf{w}^*(-k, -\omega)]^T$, and is such that

$\langle \mathbf{w}_m^*(k, \omega) \mathbf{w}_n(k', \omega') \rangle = 8\pi^2 \delta_{mn} \delta(k - k') \delta(\omega - \omega')$ and $\langle \mathbf{w}_m(k, \omega) \mathbf{w}_n(k', \omega') \rangle = 0$. The diagonal 6×6 damping matrix $\Gamma(k)$ has $\Gamma_l(k) = \gamma_l(k_l + k)$ for $1 \leq l \leq 3$ and $\Gamma_l(k) = \gamma_{l-3}(k_{l-3} - k)$ for $4 \leq l \leq 6$, while all other elements vanish. The 6×6 matrix $\mathcal{L}(k)$ has the typical Bogoliubov structure

$$\mathcal{L}(k) = \begin{pmatrix} M(k) & Q \\ -Q^* & -M^*(-k) \end{pmatrix}, \quad (13)$$

in terms of the 3×3 matrices $M(k)$ and Q whose elements (for $1 \leq m, n \leq 3$) are given by

$$\begin{aligned} M_{mn}(k) &= [\varepsilon_m(k_m + k) - \omega_m - i\gamma_m(k_m + k)/2] \delta_{m,n} \\ &+ 2 \sum_{rt} g_{1D}^{mnrt} \delta_{m,n+r-t} e^{i(\theta_r - \theta_t - \theta_m + \theta_n)} \sqrt{\rho_r^o \rho_t^o} \\ Q_{mn} &= \sum_{rt} g_{1D}^{mnrt} \delta_{m+n, r+t} e^{i(\theta_r + \theta_t - \theta_m - \theta_n)} \sqrt{\rho_r^o \rho_t^o}. \end{aligned}$$

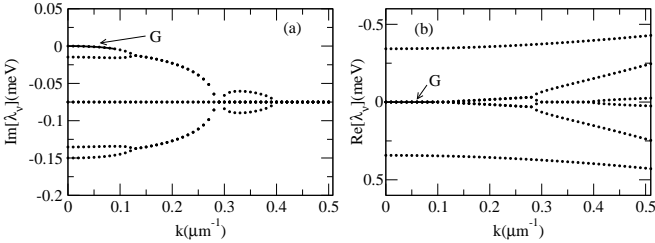


FIG. 2: Imaginary (a) and real (b) parts of the Bogoliubov excitation spectrum around the mean field steady-state. Solid line indicates the Goldstone branch. Pump-intensity as at the dotted line in Fig.1b. Same cavity parameters as in Fig.1.

The eigenvalues of the $\mathcal{L}(k)$ matrix give the excitation spectrum $\lambda_\nu(k)$ of our system around the mean-field steady-state solution. An example of such a spectrum is plotted in Fig.2. Dynamical stability of the mean-field solution requires that for all branches $\text{Im}[\lambda_\nu(k)] < 0$ for all values of k . As the mean-field solution (9) spontaneously breaks the $U(1)$ signal/idler phase symmetry $\theta_{s,i} \rightarrow \theta_{s,i} \pm \Delta\theta$ of the motion equation (3), a Goldstone branch is necessarily present. For clarity, it will be denoted in the following by the index $\nu = G$. Its main property is that its dispersion $\lambda_G(k)$ at $k = 0$ is exactly $\lambda_G(k = 0) = 0$ ¹. The behavior of this eigenvalue $\lambda_G(k)$ in the neighborhood of $k = 0$ is crucial for the long-distance properties of our system. Dynamical stability and analyticity^{1,27} arguments guarantee that for $k \rightarrow 0$ one can expand

$$\text{Im}[\lambda_G(k)] \simeq -k^2/2a, \quad (14)$$

with a strictly positive coefficient $a > 0$: differently from zero-sound in equilibrium Bose gases, the Goldstone mode is here a diffusive, non-propagating mode^{26,28}.

Note that this result, being based on symmetry arguments, does not depend on the restriction of our model to

a single polarization state per subband. Explicite inclusion of all polarization states would simply increase the dimension of \mathcal{L} to 12×12 . More Bogoliubov branches would then appear in fig.2 but no significant changes would affect the nature nor the dispersion relation of the Goldstone mode, which (as we shall see in the next section) is the only responsible for the long-distance coherence properties of the emission.

VI. FIRST ORDER CORRELATION FUNCTION

The first-order spatial coherence of the parametric emission is determined by the spatial coherence of the in-cavity polaritons^{7,29} (added ref. to baas). In the Wigner representation, this can be written for $x_1 \neq x_2$ as:

$$g_s^{(1)}(x_1 - x_2) = \langle \phi_s^*(x_1, t) \phi_s(x_2, t) \rangle_W. \quad (15)$$

Neglecting in (10) the density fluctuations $\delta\rho_j$ which do not contribute to long-distance properties, and expanding higher order correlations by means of the Wick theorem for Gaussian stochastic variables²⁰, one obtains:

$$g_s^{(1)}(x_1 - x_2) = \rho_s^o e^{ik_s(x_2 - x_1)} e^{-\chi_s(x_1 - x_2)}. \quad (16)$$

where the phase-phase correlation function is defined as:

$$\chi_s(x_1 - x_2) = \frac{1}{2} \langle [\delta\theta_s(x_1, t) - \delta\theta_s(x_2, t)]^2 \rangle_W. \quad (17)$$

This can be evaluated using (11) and (12):

$$\chi_s(x) = \frac{1}{32\pi^2 \rho_S^o} \sum_{\nu\mu} \int d\omega dk \frac{(1 - e^{ikx}) \bar{\Gamma}_{\nu\mu}(k)}{[\omega - \lambda_\nu^*(k)][\omega - \lambda_\mu(k)]}, \quad (18)$$

in terms of the matrix elements

$$\bar{\Gamma}_{\nu\mu}(k) = P^\dagger B_\mu(k) \Gamma(k) B_\nu^\dagger(k) P. \quad (19)$$

The vector P is defined as $P = (1, 0, 0, -1, 0, 0)^T$ and the matrices $B_\nu(k)$ are the projectors on the eigenspace corresponding to the eigenvalue $\lambda_\nu(k)$. The frequency integral in (18) can then be performed closing the integration contour in the complex plane:

$$\chi_s(x) = \frac{i}{16\pi \rho_S^o} \sum_{\nu\mu} \int dk (1 - e^{ikx}) \frac{\bar{\Gamma}_{\nu\mu}(k)}{\lambda_\nu^*(k) - \lambda_\mu(k)}. \quad (20)$$

As usual, the large distance properties are determined by the $k \approx 0$ region, and the dominant contribution comes from the Goldstone mode, that is for $\nu = \mu = G$. A simple analytical expression can be obtained by keeping only this mode, then approximating the smooth function $\bar{\Gamma}_{GG}(k)$ with its $k = 0$ value $\bar{\Gamma}_{GG}^o$ (of the order of the γ 's), and finally extending the integral to infinity. This results in an asymptotic exponential decrease

$$g_s^{(1)}(x) \propto e^{-|x|/\ell_c}, \quad (21)$$

with a coherence length ℓ_c equal to

$$\ell_c = \frac{16 \rho_s^0}{a \bar{\Gamma}_{GG}^0}. \quad (22)$$

In Fig.3, ℓ_c is plotted as a function of the pump power. Its behaviour closely follows the one of the signal density ρ_s^0 so that ℓ_c goes to 0 at the edges of the OPO region, and has its maximum in the middle. This prediction can be compared to the numerical results of a full Monte Carlo simulation of the Wigner equation as reported in Ref.7. The agreement is good and the small quantitative discrepancy is mostly due to the three-mode expansion performed here, which does not take into account the upper polariton.

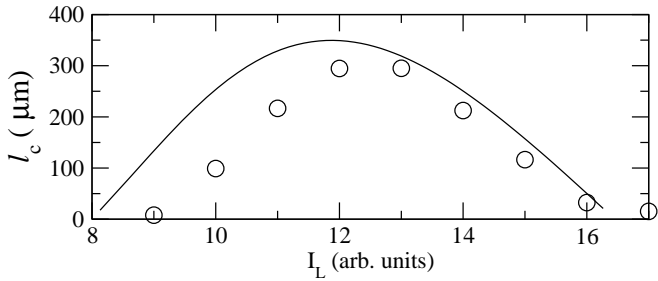


FIG. 3: Analytical prediction (22) (solid) and QMC data (circles) for the coherence length as a function of the pump power. Same cavity parameters as in Fig.1.

For a given value of the mean-field interaction energy $g\rho_j$ and all detuning and cavity parameters kept fixed, the coherence length has the remarkable scaling $\ell_c \propto 1/g$. The extremely high value of the excitonic nonlinearity implies that the effect of quantum fluctuations is strongly enhanced as compared to OPOs based on conventional nonlinear optical media^{6,12,25,30}. In particular, one can observe in Fig.3 that the predicted coherence length is of the order of hundred microns for realistic experimental parameters, which means that it should be within experimental reach with the current semiconductor technology.

As a final point, it is very instructive to compare the non-equilibrium formula (22) with the one for a degenerate 1D Bose gas of density n at equilibrium. The symmetry which is spontaneously broken is in fact the same $U(1)$ in the two cases²⁶. While at $T = 0$ the equilibrium system shows a power law decay of correlations, an exponential decay is recovered at finite T , with a coherence length given by¹¹:

$$\ell_c^{eq} = \frac{2n\hbar^2}{k_B T m} \quad (23)$$

The dependence on the density is the same in the equilibrium and non-equilibrium cases, while the role of the

temperature T is played in the non-equilibrium case by the noise associated to damping. Another, more striking, difference concerns the free boson mass m , which is replaced in the non-equilibrium case by the parameter a defined in (14), i.e. the inverse of the second derivative of the *imaginary* part of the Goldstone mode dispersion.

VII. CONCLUSIONS

In conclusion, we have developed an analytical theory which is able to describe the long-distance phase coherence of the light emitted by a one-dimensional optical parametric oscillator above threshold. Because of the reduced dimensionality, quantum fluctuations turn out to be able to destroy the long-range order. At long distances, the coherence function shows an exponential decay with a coherence length ℓ_c inversely proportional to the nonlinear coupling constant.

This result is very general and holds for any kind of one-dimensional parametrical oscillator, as well as for other examples of non-equilibrium phase transitions in reduced dimensionality. We have concentrated our attention on semiconductor photonic wires in the strong coupling regime simply because such systems appear as very promising candidates to experimentally investigate this physics. The extremely large value of the exciton-exciton interactions corresponds in fact to a value of ℓ_c short enough to be within reach of the current semiconductor technology.

In addition to their interest for the fundamental physics of pattern formation and non-equilibrium phase transitions, the conclusions of the present paper may also have significant consequences for device applications of OPOs, as quantum fluctuations provide an intrinsic limitation to the long distance phase coherence that can be obtained even in the absence of other decoherence and disorder effects.

VIII. ACKNOWLEDGEMENTS

Continuous stimulating discussions with C. Ciuti, J. Tignon, C. Diederichs, and A. Rosso are warmly acknowledged. This research has been supported financially by the FWO-V projects Nos. G.0435.03, G.0115.06, and the Special Research Fund of the University of Antwerp, BOF NOI UA 2004. M.W. acknowledges financial support from the FWO-Vlaanderen in the form of a “mandaat Postdoctoraal Onderzoeker”.

¹ M. C. Cross and P. C. Hohenberg, Rev. Mod. Phys. **65**, 851 (1993).

² L.A. Lugiato, M. Brambilla and A. Gatti, Adv. At. Mol. Opt. Phys. **40**, 229 (1998).

³ K. Staliunas, *Transverse Patterns in Nonlinear Optical Resonators* (Springer, 2003).

⁴ D. F. Walls and G. J. Milburn, *Quantum Optics* (Springer, 1994).

⁵ L.P. Pitaevskii and S. Stringari, *Bose-Einstein Condensation*, Clarendon Press Oxford (2003).

⁶ A. Gatti, L. Lugiato, Phys. Rev. A **52**, 1675 (1995).

⁷ I. Carusotto and C. Ciuti, Phys. Rev. B **72**, 125335 (2005).

⁸ for an introduction, see L. E. Reichel, *A Modern Course in Statistical Physics*, University of Texas Press (1980).

⁹ *Phase transitions and critical phenomena*, vol.17 (Statistical mechanics of driven diffusive systems), eds. C. Domb and J.L. Lebowitz, Academic, Neq York (1989).

¹⁰ V.N. Popov, *Functional Integrals in Quantum Field Theory and Statistical Physics*, Reidel Dordrecht (1983).

¹¹ Y. Castin, J. Phys. IV France, **116**, 89 (2004) and references therein.

¹² R. Zambrini, M. Hoyuelos, A. Gatti, P. Colet, L. Lugiato, and M. San Miguel, Phys. Rev. A **62**, 063801 (2000).

¹³ K. Staliunas, cond-mat/0001436; K. Staliunas, Phys. Rev. E **64**, 066129 (2001).

¹⁴ J. Baumberg and L. Viña (Eds.) Special issue on Microcavities, [Semicond. Sci. Technol. **18**, S279 (2003)].

¹⁵ B. Deveaud (Ed.), Special issue on the “Physics of semiconductors microcavities”, Phys. Stat. Sol. B **242**, 2145-2356 (2005) and references therein.

¹⁶ R. M. Stevenson, V. N. Astratov, M. S. Skolnick, D. M. Whittaker, M. Emam-Ismail, A. I. Tartakovskii, P. G. Savvidis, J. J. Baumberg, and J. S. Roberts, Phys. Rev. Lett **85**, 3680 (2000).

¹⁷ R. Houdré, C. Weisbuch, R. P. Stanley, U. Oesterle, and M. Illegems, Phys. Rev. Lett. **85**, 2793 (2000).

¹⁸ G. Dasbach, C. Diederichs, J. Tignon, C. Ciuti, Ph. Rousignol, C. Delalande, M. Bayer, and A. Forchel, Phys. Rev. B **71**, 161308(R) (2005).

¹⁹ G. Panzarini and L. C. Andreani, Phys. Rev. B **60**, 16799 (1999)

²⁰ C.W. Gardiner and P. Zoller, *Quantum Noise* (Springer, 2004).

²¹ T.-L. Ho, Phys. Rev. Lett. **81**, 742 (1998).

²² I. A. Shelykh, Yuri G. Rubo, G. Malpuech, D. D. Solnyshkov, and A. Kavokin, Phys. Rev. Lett. **97**, 066402 (2006).

²³ I. Carusotto and C. Ciuti, Phys. Rev. Lett. **93**, 166401 (2004).

²⁴ D.M. Whittaker, Phys. Rev. B **71**, 115301 (2005)

²⁵ M. Wouters and I. Carusotto, cond-mat/0607719.

²⁶ M. Wouters and I. Carusotto, cond-mat/0606755.

²⁷ T. Kato, *Perturbation theory for linear operators* (Springer-Verlag, 1984).

²⁸ While the present paper was under review, similar results for a different but related model have appeared in M. H. Szymanska, J. Keeling, P. B. Littlewood, Phys. Rev. Lett. **96**, 230602 (2006)

²⁹ A. Baas, J.-Ph. Karr, M. Romanelli, A. Bramati, and E. Giacobino, Phys. Rev. Lett. **96**, 176401 (2006)

³⁰ R.L. Sutherland, *Handbook of nonlinear optics* (Marcel Dekker, 2003).

³¹ This is exact as long as the confinement in the z direction is stronger than the one in the y direction and the leakage of the photonic wavefunction in the air surrounding the structure can be neglected. For typical confinement sizes L_y of the order of a few microns, these approximation are very accurate¹⁹.

³² The Wigner approach gives accurate results provided the weak-interaction condition $\gamma_j \gg g k_{\text{UV}}/L_y$ is satisfied, k_{UV} being the UV cut-off of the theory, to be taken larger than any characteristic wavevector in the problem.

³³ The k -dependence of the final density of states and of the tunneling matrix element through the DBR cavity mirrors can be safely neglected as long as the characteristic wavevectors $k_{y,j}$ and $1/\ell_c$ of the in-cavity polaritons are well inside the DBR reflection window.